Utilization of the Transient Liquid Crystal Technique for Film Cooling Effectiveness and Heat Transfer Investigations on a Flat Plate and a Turbine Airfoil

U. Drost, A. Bölcs
Swiss Federal Institute of Technology
EPFL-LTT
Lausanne, Switzerland

A. Hoffs
ABB Power Generation Ltd.
Gas Turbine Development
Baden, Switzerland

ABSTRACT

The transient liquid crystal technique has been used to measure film cooling effectiveness and heat transfer on a flat plate in a free jet, and a turbine airfoil in a linear cascade. A multiple-test regression method has been developed for the data reduction, considering a transient coolant temperature evolution. Flat plate film cooling was investigated for a single row of 35° inclined holes at Mach numbers of 0.3 and 0.5, and two turbulence intensities. Downstream of injection heat transfer was increased in-between the holes due to enhanced turbulence caused by the shearing of the coolant and the mainstream. At higher turbulence intensity the range of blowing ratios was broader as lift-off was delayed. Film cooling measurements on the airfoil were conducted at engine-representative flow conditions. A maximum effectiveness of 0.3 behind injection was observed on the suction side, with slightly higher values for a double row in comparison to a single row configuration. Due to a high coolant momentum, the effectiveness on the pressure side was very low at about 0.05 for a single row configuration.

NOMENCLATURE

c_p specific heat capacity [J/kgK]
d cooling hole diameter [mm]
f frequency [Hz]
DR density ratio ρ_c/ρ_g
G blowing ratio $\rho_c u_c/\rho_g u_g$
I momentum flux ratio $\rho_c u_c^2/\rho_g u_g^2$
l_h hole length [mm]
L airfoil chord [mm]
L_x Integral length scale[mm]
M Mach number
Me turbulence grid meshsize [mm]
p hole pitch [mm]
Re Reynolds number
R_z surface roughness DIN4768 [µm]
s surface distance from leading edge [mm]
T temperature [K]
t time [s]
Tu turbulence intensity [%]
x axial coordinate [mm]

y coordinate normal to the surface [mm]
z spanwise coordinate [mm]

Greek
α heat transfer coefficient [W/m²K]
β dimensionless heat transfer coefficient
η film cooling effectiveness $\left(T_{aw} - T_{rg}\right)/\left(T_{tc} - T_{tg}\right)$
θ temperature ratio $\left(T_{tg} - T_{tc}\right)/\left(T_{rg} - T_w\right)$
λ thermal conductivity [W/mK]
Λ thermal diffusity [m²/s]
ρ density [kg/m³]
φ streamwise injection angle [°]
γ spanwise injection angle [°]

Indices
c coolant
i initial
g free-stream
k roughness height
r recovery
s static
t total
w wall
L based on chord length
1 inlet
2 exit

INTRODUCTION

The power output and efficiency level of a gas turbine improves by increasing the turbine inlet temperature. Since these temperatures exceed the highest allowable blade material temperature the blades have to be cooled to guarantee safe operating conditions. Discrete hole film cooling is an effective way to achieve this objective, provided that the thermal boundary conditions are known accurately. As numerical predictions of three-temperature convection situations on complex geometries as turbine airfoils are not yet sufficiently reliable for design purposes experimental information is urgently needed. Hence, an experimental heat transfer research program has been initiated at the EPFL, and two-temperature situation convection results on flat plate,

cylinder and airfoil geometries have been recently reported in Häring et al., (1995, 1996) and Hoffs et al. (1995, 1996).

The objective of the present work is to show the utilization of the transient liquid crystal technique in film cooling situations on complex geometries. An evaluation procedure is presented allowing the deduction of both the film cooling effectiveness and heat transfer coefficients from ensembles of 6 to 8 tests conducted at identical aerodynamic, but varying coolant injection temperatures. A similar evaluation procedure has been reported by Wang et al. (1994) being named the temperature matching method. Regression analysis was used to select values of the heat transfer coefficient and adiabatic wall temperature to minimize the sum of squared differences between the measured surface temperature and a semi-infinite transient conduction model. Vedula and Metzger (1991) presented an evaluation procedure based on two distinct measurements where the two unknowns are obtained from a double-equation system. Their measurement setup did not allow true step-changes in the applied fluid temperatures, which was accounted for by using a series of steps for the solution of the semi-infinite model.

In the present paper, a flat plate with a single row of $35°$ inclined holes has been investigated for Mach numbers of 0.3 and 0.5, at low and high mainstream turbulence intensities. The blowing ratios were varied between 0.3 and 1.5 at a density ratio of 1.6, which was obtained with foreign gas injection. A similar film cooling geometry has been used by Ammari et al. (1990), Sinha et al. (1991) and Schmidt et al. (1994), and comparisons are made with results reported by these authors. Ammari et al. showed an increase in heat transfer with respect to an uncooled case for a density ratio of 1.52. Sinha et al. measured film cooling effectiveness at various density ratios, and Schmidt et al. studied the influence of compound angle on effectiveness.

Subsequently, the transient liquid crystal technique was used for effectiveness and heat transfer measurements on a turbine airfoil at engine-representative flow conditions. On the suction side, single and double row injection into an accelerating boundary layer are compared, while pressure side film cooling was only done for one row.

Theory

The local heat flux in the film cooling situation can be described as follows,

$$q = \alpha_f \left(T_{aw} - T_w \right) \qquad (1)$$

where the convection coefficient is based on the unknown adiabatic wall temperature that depends on the supply temperatures of the main and secondary streams and the degree of mixing. In dimensionless form this temperature becomes the film cooling effectiveness, defined for flow with dissipation as (Teekaram et al., 1990),

$$\eta = \frac{T_{aw} - T_{rg}}{T_{tc} - T_{tg}} \qquad (2)$$

The two unknowns of such a three-temperature situation are thus the heat transfer coefficient α_f and the film cooling effectiveness, η. Both values are functions of the aerodynamic character of the flow field alone (Vedula and Metzger, 1991).

In the present work, these two unknowns are determined by conducting transient tests where the model is suddenly exposed to a steady mainstream. The transient heating of the surface is monitored by the color play of a liquid crystal coating. Initially the model is at a homogenous temperature, so that for short testing times the transient heating near the surface can be described by one-dimensional semi-infinite heat conduction. The governing differential equation and appropriate boundary conditions are then,

$$\frac{\partial^2 T}{\partial y^2} = \frac{1}{\Lambda} \frac{\partial T}{\partial t} \qquad (3)$$

$$\lim_{y \to \infty} T(y,t) = T_i \qquad (4)$$

$$T(y,0) = T_i \qquad (5)$$

$$-\lambda \frac{\partial T(0,t)}{\partial y} = \alpha_f \left(T_{aw} - T(0,t) \right) \qquad (6)$$

In the experiments a complication was introduced, since a true step change of the coolant temperature was not possible due to heat exchange in the supply tubing and plenum chamber. Thus, the adiabatic wall temperature became a function of time, which had to be accounted for in the evaluation. The measured coolant temperature distribution was approximated by a power series of the following form,

$$T_{tc}(t) = \sum_{n=0}^{N} A_n \frac{t^n}{\Gamma(n+1)} \qquad (7)$$
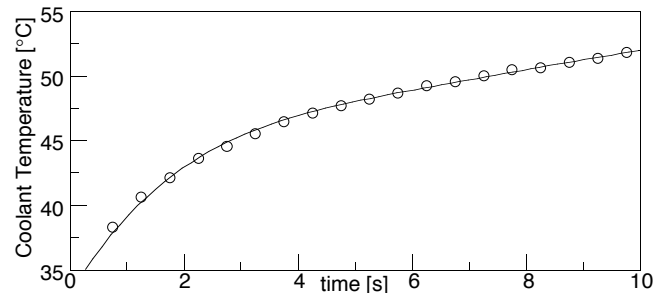
usually chosen of 4th to 5th order (Fig. 1).

Fig.1 Coolant temperature evolution and 5th order fit

Using this closed expression for T_{tc}, an analytical solution to the equations (3) to (7) was obtained for y=0 using the Laplace transform method,

$$T_w - T_i = \left(T_{rg} - \eta T_{tg} - T_i \right) \left[1 - e^{\beta^2} \mathrm{erfc}(\beta) \right]$$
$$- \eta \sum_{n=0}^{N} \left\{ A_n \left(\frac{\kappa}{\alpha_f} \right)^{2n} \left[e^{\beta^2} \mathrm{erfc}(\beta) - \sum_{\tau=0}^{2n} \left([-2\beta]^\tau \, i^\tau \mathrm{erfc}(0) \right) \right] \right\} \qquad (8)$$

with

2

$$\kappa = \frac{\lambda}{\sqrt{\Lambda}} = \sqrt{\rho \cdot \lambda \cdot c_p}$$

$$\beta = \frac{\alpha_f \sqrt{t}}{\kappa}$$

Eq. (8) contains the two unknowns α_f and η, which are deduced via a regression analysis similar to that proposed by Wang et al. (1994). Least squares fitting of the model equation to the wall temperature rise yields the two unknowns. Wang measured the wall temperature during a single experiment with large-band liquid crystals. In theory two points of the temperature history would be sufficient to determine the two unknowns at each point of the surface. However, the measurement uncertainty can be significantly reduced by adding additional points to the evaluation and by applying regression analysis.

In the present work, a single layer of narrow-band liquid crystal was used to avoid additional complications related to the view angle dependency of large-band liquid crystals. Multiple layers of narrow-band liquid crystals could not be employed, because the hue signals recorded by the image processing system did not allow a clear identification of each layer.

According to Vedula and Metzger (1991), several experiments can be evaluated together, if they are conducted under identical aerodynamic conditions but different flow temperatures. Forth et al. (1985) on the other hand mentioned that a constant flow field can only be maintained when both the freestream and injection temperatures are kept constant and only the wall temperature is altered. However, Ligrani and Camci (1985) conducted film cooling tests in compressible, variable property flow, where the coolant temperature variation changed the density ratio. They kept either the blowing ratio, momentum flux ratio or velocity ratio constant and observed alteration in η within +/-10%. The best agreement with constant property measurements was found when the blowing ratio was maintained.

For the present study usually 6 to 8 tests were carried out at identical blowing ratios, total temperatures and liquid crystal temperatures, whereas the coolant injection temperature was varied in a range of 0°C to 50°C. These test ensembles were then evaluated together by fitting eq. (8) through the measured points using a least squares regression procedure. Typical variations of I and DR with θ for one ensemble are presented in Fig. 2, which shows that the maximum differences are in the order of 8 %.
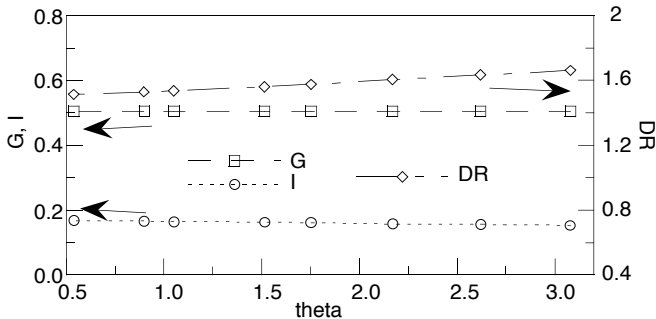

Fig. 2 Variation of G, I, and DR with θ

Measurement uncertainties

Using only two transient tests for the data evaluation reduces the evaluation analysis to a simple 2 equation problem with 2 unknowns. For such a constellation, typical uncertainties in η and α_f can be determined according to Kline and McClintock (1953), considering the following major contributors to the uncertainty,

$$T_w = 0.3 \text{ K}$$
$$T_i = 0.5 \text{ K}$$
$$T_g = 0.5 \text{ K}$$
$$T_c = 1 \text{ K}$$

$$\lambda = 3 \text{ \%}$$
$$\Lambda = 3 \text{ \%}$$
$$t = 2/25 \text{ s}$$

Hence, for two tests uncertainty in heat transfer coefficient yields a value of about 10%, and in local effectiveness a value of 20% at $\eta=0.1$, decreasing to 6% for $\eta=0.3$. These values were considered to be too high for systematic film cooling parameter studies and consequently the described multiple-test regression procedure was implemented.

For this regression analysis the determination of uncertainty values revealed to be a rather difficult task due to the non-linear character of the regression model. The only direct measure of regression quality is given by the RMS deviations of the actual measured wall temperatures to those obtained from the model, which are of the order of 0.5 K for gas to initial temperature differences of 30 K. However, this information tells nothing about the uncertainties in η and α_f.

Hence, for the regression method an uncertainty analysis was carried out in two steps. A statistical analysis was conducted by systematically varying the number of tests of an evaluation ensemble. Here, the decrease of average relative deviations in η and α_f was observed with increasing test numbers. For more than 5 tests, this deviation fell below 1% so that the ensembles were considered to be in statistical equilibrium (Fig.3).

An uncertainty analysis according to Kline and McClintock (1953) was then carried out using the governing least squares equation derived from eq. (8), considering the contributors given above. Uncertainty in heat transfer coefficient yields a rather constant value of 6%, and in local effectiveness a value of 10% at $\eta=0.1$, decreasing to 4% for $\eta=0.3$. For laterally averaged effectiveness, uncertainty yields a value of 8% for $\eta=0.3$.
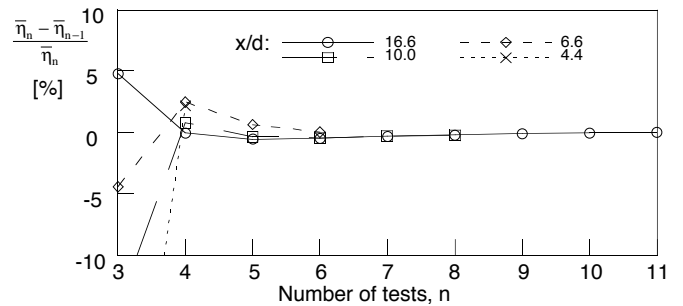

Fig. 3 Average relative error in η as a function of test numbers

The effect of the transient coolant temperature distribution (Fig. 1) during the tests with respect to evaluations conducted at constant average coolant temperatures was assessed to

be up to 8% for the heat transfer coefficient and up to 16% for η.

FLAT PLATE
Test Facility/Measuring Equipment

The flat plate measurements were conducted in a free jet test facility with a nozzle diameter of 150 mm as shown in Fig. 4. The test facility is supplied from a continuously running air source delivering a mass flow up to 10 kg/s with a maximum pressure ratio of 3.5. Total pressure and total temperature were measured in the settling chamber for low turbulence tests. When the turbulence grid was attached to the nozzle, a total pressure probe was used downstream of the screen.
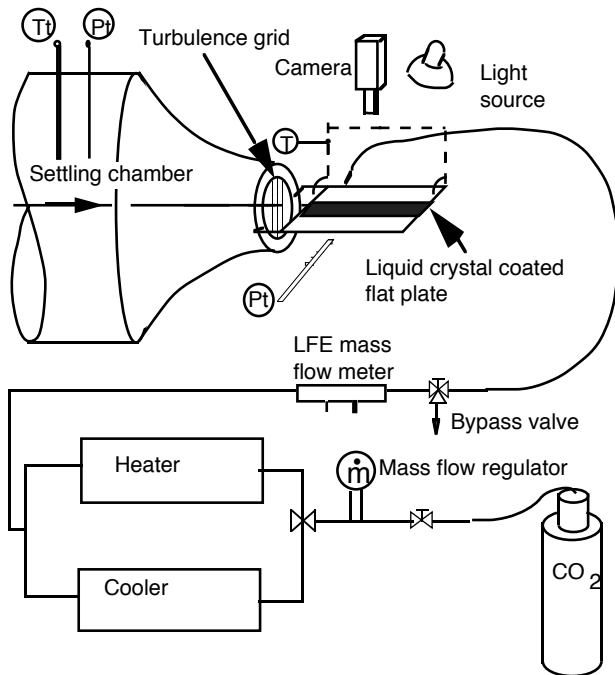
Fig.4 Free jet test facility

The measurements were conducted on a flat plate (Fig. 5) made out of perspex. Its leading edge was located 0.35 free-jet diameters downstream of the nozzle and the trailing edge 2.35 diameters. Flowfield surveys showed negligible expansion of the free-jet in this range. The film cooling geometry consisted of one row of 14 holes with diameter d=1.8 mm inclined with 35° in the flow direction from the surface. The holes were located 36 hole diameters from the leading edge, the lateral spacing of the holes was 3 hole diameters, and the hole length 3.5 hole diameters. The injection system had a feeding chamber in the model itself and supply of the coolant from one side similar to a blade. A special convergent form according to the manifold model of Bajura (1971) was given to the chamber to insure an even coolant distribution to the holes. The cooling holes were sharp entry and the plenum entry section was 60 hole sections. The coolant properties were measured in the plenum chamber by means of two thermocouples and a pressure tapping. Six thermocouples were distributed along the surface to measure the initial temperature of the plate. A strip of 10 mm large sand paper was pasted onto the leading edge to provoke a laminar-turbulent transition at this location, selected according to the

critical roughness Reynolds number of $Re_{k,\infty} = 680$ (Doenhoff and Horton, 1956). The coolant mass flow rate was metered with a Meriam Instr. laminar flow element and additionally with a Brooks Inc. mass flow regulator.

The flat plate was mounted on a turning mechanism which allows its sudden exposure to the main flow in less than 0.1s. Pivoting the plate activated a bypass valve which fed the coolant into the plate plenum chamber.
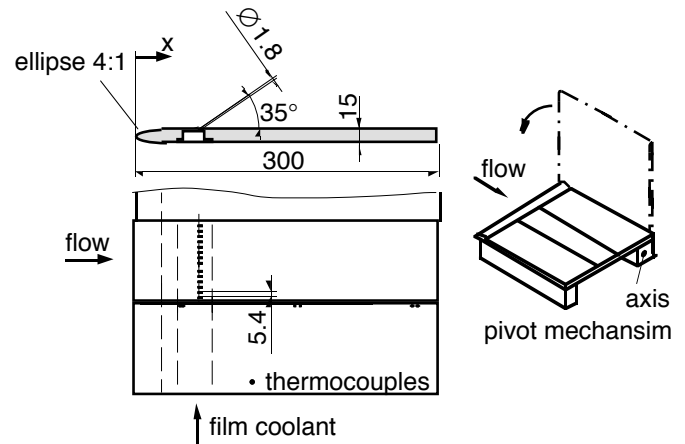

Fig. 5 Flat Plate

Variations in plate Reynolds number were achieved with different inlet flow rates and total pressures whereas the mainstream temperature remained approximately constant at 48°C. Foreign gas injection using CO_2 was employed to achieve a density ratio of 1.6, as proposed by Teekaram et al. (1989).

Measurement Technique

The present image processing system is based on the hue capturing technique using an automated image processing system as already described in Häring et al. (1995). Since the color play of the liquid crystals is taken under a certain viewing angle the original surface coordinates are correlated numerically with the camera picture to correct the image distortion.

Narrow-band microencapsulated thermochromic liquid crystals were used for the tests, which were applied to the surface with a precision airbrush, and covered with a thin layer of binder to protect the capsules. Due to the spraying process the surface always exposes a certain roughness so that polishing of the surface with very fine sandpaper became inevitable to obtain smooth and repeatable surface conditions. The surface roughness was measured with a Perthen SP6 profilometer and a piezo-electrique measuring sensor (RFHTB50, 0-50 μm) on various locations at the plate. For the polished smooth surface an average roughness value of R_z=15 μm (R_a=1.7 μm) was found.

TURBULENCE MEASUREMENTS
Turbulence Generating Grid

In order to obtain a high turbulence level, a square array biplane grid constructed with rectangular bars has been inserted. The turbulence grid had a meshsize of 15 mm, a mesh- to barsize ratio of 5, and was placed 8.5 mesh sizes

4

upstream of the injection location to achieve a high turbulence intensity, albeit with a considerable degree of anisotropy.

Turbulence Measurement Data Reduction

Turbulence intensity decay and length scale growth were measured with a Dantec 55M01 constant temperature anemometer and a standard single hot-wire probe. A high sampling frequency of 40 kHz was chosen to resolve small eddy structures and the sampling time was 5 seconds. The turbulence data was low-pass filtered at 16 kHz to avoid aliasing errors due to contributions from higher frequencies. The probe was calibrated in situ at different mainstream velocities. The calibration curve was then obtained by fitting a fourth order least-squares curve of the density-velocity product as a function of the probe voltage. Fast Fourier transforms were applied to the measured velocity samples and, using the Wiener-Khinchin Theorem (Bendat and Piersol, 1985) the autocorrelation was calculated. Integration of the latter until the first zero-passage led to the integral length scale. The uncertainties for the turbulence level and scale are 0.5% and 2 mm, respectively.

Turbulence Measurement Results

Turbulence intensity in the clear free-jet was measured to 1.4%, accompanied by a high integral length scale of 30 mm. The turbulence intensity decay downstream of the grid is shown in Fig. 6 and compares very well to the correlation from Baines and Peterson (1951). At the injection location, the Tu value was 8% and at the leading edge 15%. Length scale growth was weak yielding a lengthscale of 9 mm at injection location.
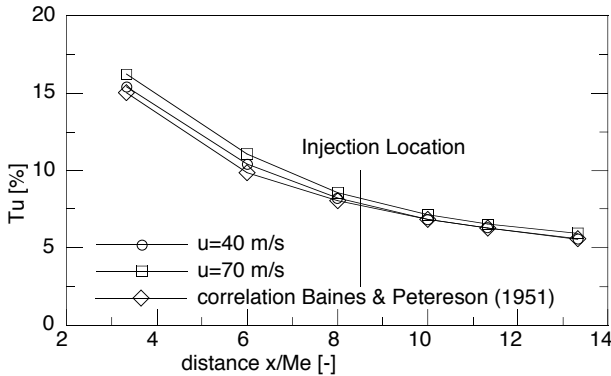

Fig. 6 Turbulence intensity decay downstream of grid

RESULTS AND DISCUSSION FLAT PLATE

The film cooling measurements on the flat plate had two objectives. First, the relatively straight-forward experimental set-up allowed the preparation and testing of the additional measuring devices. Due to a large number of openly available research work on film-cooled flat plates it was then possible to compare and validate the present measurements.

The range of experimental parameters which were varied in the current study is listed in table 1.

M	G	I	DR	δ_1/d	Tu [%]
0.3	0.3	0.06	1.6	0.127	1
0.3	0.5	0.16	1.6	0.127	1
0.3	0.7	0.31	1.6	0.127	1
0.3	1.0	0.63	1.6	0.127	1
0.3	1.5	1.36	1.6	0.127	1
0.3	0.3	0.06	1.6	0.127	high
0.3	0.5	0.16	1.6	0.127	high
0.3	1.0	0.63	1.6	0.127	high
0.3	1.5	1.36	1.6	0.127	high
0.5	0.3	0.06	1.6	0.114	1
0.5	0.3	0.06	1.6	0.114	high
0.5	0.7	0.30	1.6	0.114	1
0.5	0.7	0.30	1.6	0.114	high

Table 1 Flat plate test conditions

The boundary layer displacement thicknesses given in table 1 were calculated with a correlation from Schlichting (1968) for turbulent boundary layers,

$$\delta_0 = 0.37 \frac{x}{Re_x^{1/5}}$$

$$\delta_1 = \frac{\delta_0}{8} \tag{9}$$

FILM COOLING EFFECTIVENESS
Effect of blowing/momentum flux ratio

The complete surface effectiveness distributions were integrated over 27 mm in the flow center to obtain laterally averaged values $\overline{\eta}$. Fig. 7 shows the evolution of $\overline{\eta}$ for different blowing ratios at a Mach number of 0.3 and Tu=1.4 %. Some data scatter in the immediate vicinity of injection is due to a lack of optical resolution of the steep temperature gradients in this region. For low blowing ratios $\overline{\eta}$ has a maximum near the holes and monotonically decreases further downstream. Jet lift-off occurs at a blowing rate of about 1, which flattens the effectiveness in vicinity to the holes, but produces rather high values further downstream. Highest overall effectiveness is observed at G=0.7.
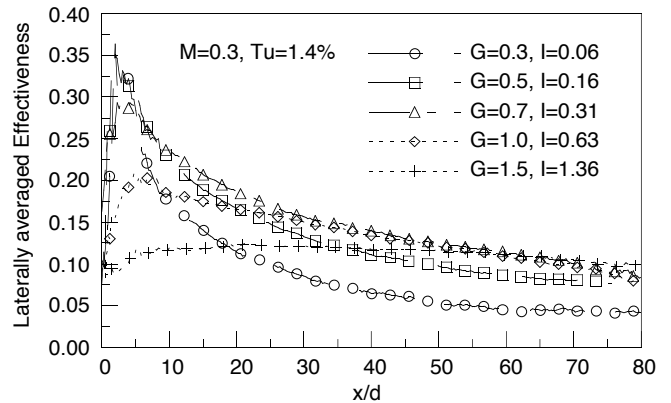

Fig. 7 Laterally averaged effectiveness at various blowing ratios

The excellent resolution of the measurements is illustrated by spanwise effectiveness distributions at different axial positions for G=0.5 shown in Fig. 8. Downstream of the hole centerlines effectiveness values close to unity are obtained at a position of x/d=3, whereas in-between the holes no cooling effect is visible. As mixing of the jets occurs through the turbulent boundary layer, the effectiveness peaks gradually level out to a value of 0.2 at x/d=17.
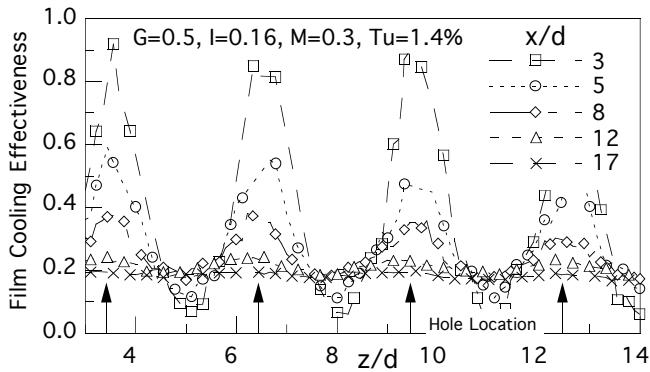
Fig. 8 Spanwise effectiveness distribution

Effect of mainstream turbulence

The influence of the turbulence intensity on $\bar{\eta}$ is depicted in Fig. 9 for different blowing ratios. For blowing ratios lower than 1, $\bar{\eta}$ is lower for the high turbulence cases due to stronger mixing in the boundary layer. However, when the jets start to detach from the surface for a blowing ratio of about 1, the high turbulence cases perform gradually better, for G=1.0 close to the holes and for G=1.5 also further downstream. At high turbulence, a part of the coolant mass flow seems to be shedded from the detaching jets increasing its dispersion into the boundary layer. Schmidt and Bogart (1996) conducted flat plate film cooling measurements at three turbulence intensities (0.3%, 10%, 17%) and observed the same phenomena.
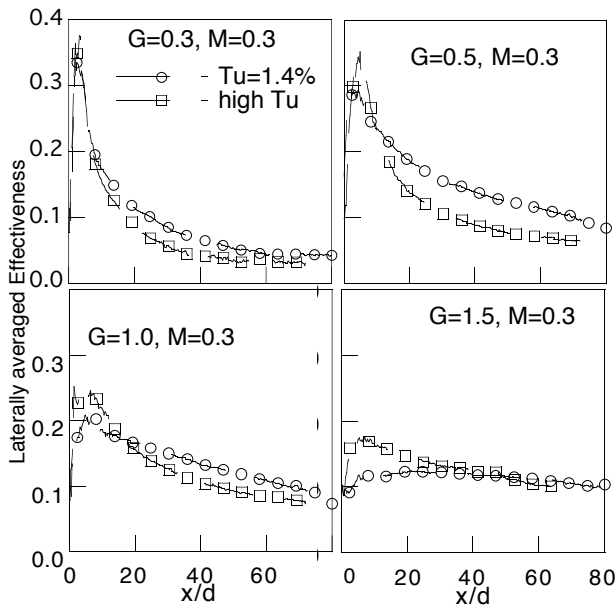

Fig. 9 Laterally averaged effectiveness at two Tu-intensities

Variation of the mainstream Mach number

Experiments were carried out at Mach numbers of 0.3 and 0.5 and blowing ratios of 0.3 and 0.7, at two turbulence intensities. In Fig. 10 is shown that from about 20 hole diameters downstream of injection the effectiveness is unaffected by the Mach number, which was also found by Liess (1975). In the near hole region however, the higher Mach number tests yield slightly higher values. However, this

difference can be probably attributed to the changing boundary layer thicknesses, which decreases with increasing Mach number. Other researcher have also found that with increasing δ_1/d the effectiveness decreased (Liess, 1975, Pederson et al., 1977, Foster and Lampard, 1980).
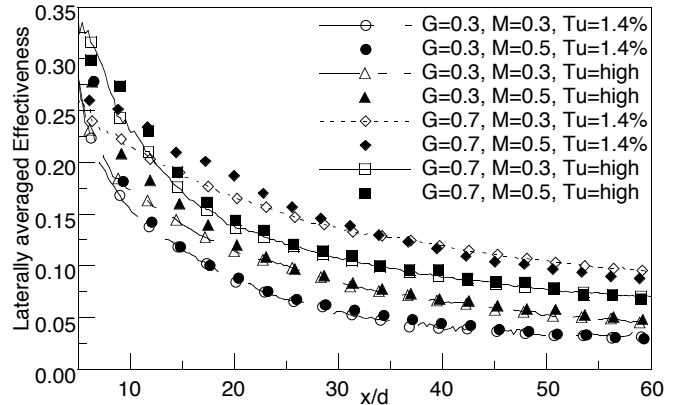

Fig. 10 Laterally averaged effectiveness at two Mach numbers

Comparison of effectiveness to literature results

Comparisons of centerline effectiveness results, η_c, were made to data by Sinha et al. (1991) and Schmidt et al. (1994), who used injection geometries similar to the present study. For both low and high blowing ratios the agreement between the results is good (Fig. 11), although the data of the present study shows a decrease of effectiveness at a slightly greater rate.
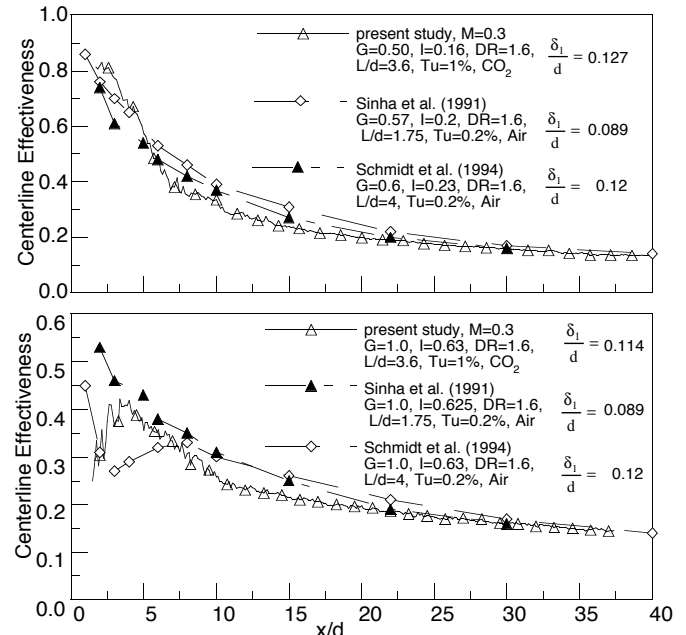

Fig. 11 Centerline effectiveness comparison with published data

The differences can be attributed to differences in freestream turbulence intensity and boundary layer thickness, which were higher in the present study. As pointed out earlier, both of these factors tend to reduce the effectiveness and thus explain the observed deviations.

FILM COOLING HEAT TRANSFER COEFFICIENT
Effect of blowing/momentum flux ratios

Laterally averaged heat transfer augmentation with respect to an uncooled baseline test without cooling holes is presented in Fig. 12, for different blowing ratios at M=0.3 and Tu=1.4%. For all except the highest blowing ratio a remarkable increase in heat transfer is limited to about 10 hole diameters downstream of injection, whereafter it decreases to a value of 1. Only for the highest blowing ratio, a maximum of 20% increase occurs at x/d=20, which indicates the reattachment location of the jets after lift-off behind injection.
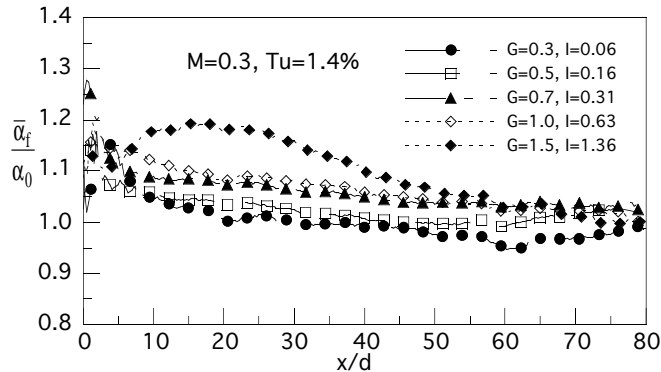

Fig. 12 Laterally averaged heat transfer augmentation

The spanwise distribution of heat transfer for G=0.5 is depicted in Fig. 13. The heat transfer is increased at locations where the edge of the jet and the mainstream interact. Such behavior was observed for all blowing ratios. Results from Eriksen and Goldstein (1974) showed the same trends.
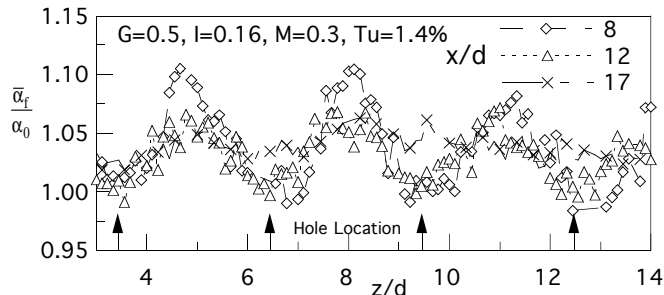

Fig. 13 Spanwise heat transfer augmentation

Comparison of heat transfer to literature results

Comparisons of laterally averaged heat transfer were done with data published by Ammari et al. (1990) who conducted film cooling heat transfer measurements at two density ratios of 1 and 1.52.

For a blowing ratio of 0.5, the present data agrees well with that by Ammari et al. (1990), whereas the rate of decrease is significantly lower at a blowing ratio of 1 (Fig. 14). This may be due to different boundary layer thicknesses and conditions. Lateral distributions shown by Ammari et al. indicated maximum heat transfer in the hole centerlines, whereas in the present study highest heat transfer was observed in-between the holes.
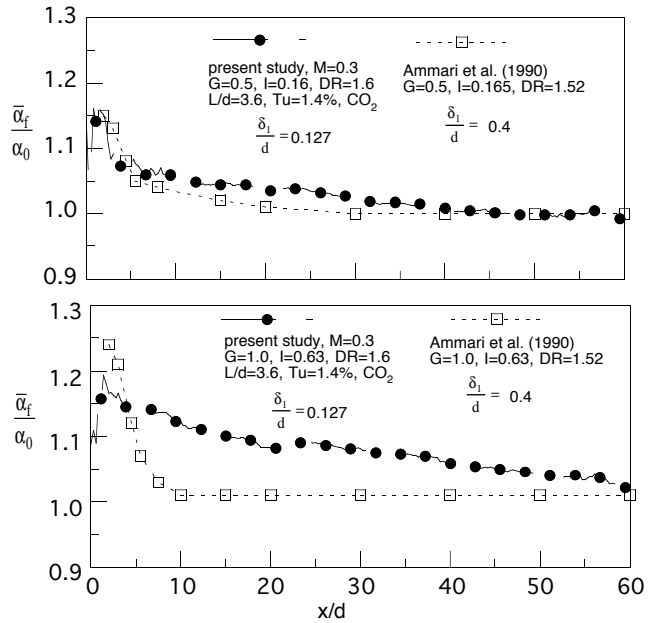

Fig. 14 Laterally averaged heat transfer augmentation comparison with Ammari et al. (1990)

TURBINE AIRFOIL
Test Facility

The measurements on the turbine airfoil were performed in a linear turbine cascade facility with five airfoils mounted onto a cylindrical disc in the 99 x 340 mm working section as shown in Fig. 15. An insertion mechanism was employed for the transient tests where a pneumatic cylinder pulls the airfoil very rapidly (below 0.1 s) through the sidewalls of the linear cascade, which has been described in Hoffs et al. (1996). For the present measurements, a new insertion system was constructed to allow film cooling on a modern airfoil geometry with a contoured endwall (Hoffs, 1996). A large cooling system was installed to pre-condition the initial and the film coolant temperatures below zero degrees Celsius.
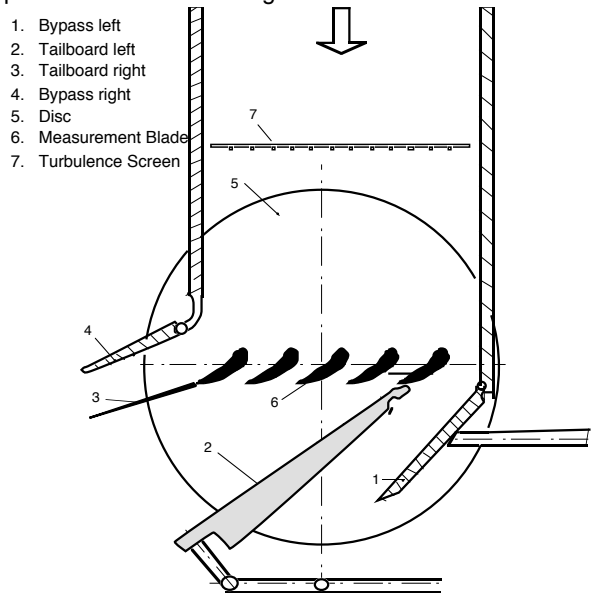

1. Bypass left
2. Tailboard left
3. Tailboard right
4. Bypass right
5. Disc
6. Measurement Blade
7. Turbulence Screen

Fig. 15 Schematic view of the linear test facility

One film cooling row was placed respectively on the pressure and the suction side close to the leading edge. Additional measurements were performed on the suction side with a double-row configuration. The dimensionless positions of the film cooling holes with respect to the geometrical leading edge are s/L_{PS}=-0.123 for the pressure side row and s/L_{SS}=0.377 for the suction side rows (Table 2). The coolant was supplied from one side to a cylindrical plenum chamber in the blade, and the film holes were sharp entry.

Geometry	s/L	φ [°]	γ [°]	p/d	l_h/d
single PS	-0.123	55	60	6.25	9.25
single SS	0.377	35	90	3.75	11.0
double SS	0.377	30	90	4.30	11.0

Table 2 Film cooling configuration airfoil

RESULTS AND DISCUSSION AIRFOIL

The measurements on the airfoil were performed at engine-representative exit Reynolds and Mach numbers of 1.5e6 and 0.8. A high turbulence intensity of 10% with a lengthscale of 13 mm at the leading edge was achieved with a grid located 10 mesh sizes upstream of the leading edge. The blowing and momentum flux ratios were 4 and 9 for the pressure side, 1 and 0.5 for the suctions side single row, and 0.78 and 0.38 for the suction side double row (Table 3).

Geometry	M_2	Re_2	G	I	DR
single PS	0.8	1.5e6	3.84	8.78	1.69
single SS	0.8	1.5e6	0.93	0.55	1.60
double SS	0.8	1.5e6	0.78	0.38	1.60

Table 3 Airfoil test conditions

In Fig. 16, the isentropic Mach number distribution is shown together with the baseline heat transfer measurements carried out without holes, which were measured at midspan. Along the suction side, there is an initially strong acceleration of the flow up to s/L = 0.45, whereafter it becomes almost uniform. Transition is observed between 0.5 and 0.8 with a turbulent boundary layer close to the trailing edge. On the pressure side the acceleration is almost constant. The heat transfer measurements indicate a laminar boundary layer which becomes transitional near the trailing edge.
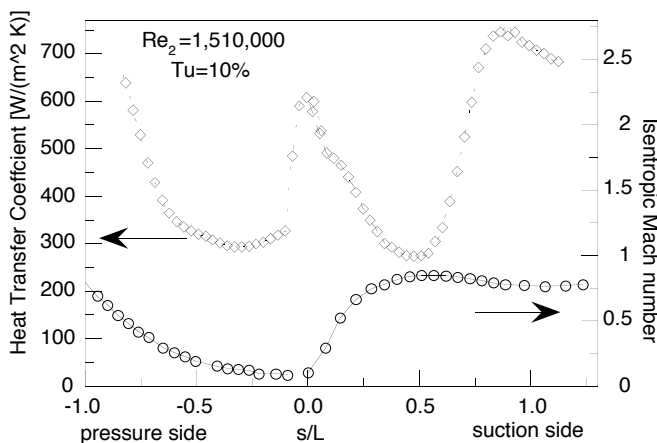

Fig. 16 Airfoil Mach number distribution and heat transfer without injection

Film cooling effectiveness results on the airfoil are shown in Fig. 17. On the suction side, a value of 0.3 is observed behind the holes with slightly higher values for the double-row configuration which is due to a better film coverage and a higher mass flow rate. For this configuration, measurements were also taken at the leading edge, and the evaluation shows the expected zero effectiveness. The effectiveness on the pressure side is very low with a short peak behind the holes, and a constant value of 0.05 further downstream.
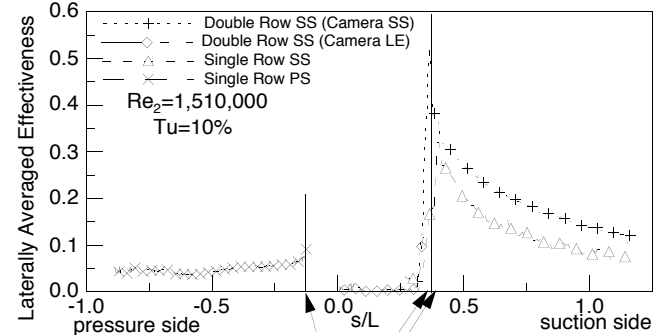

Fig. 17 Film cooling effectiveness on the vane

Film cooling heat transfer augmentation is shown in Fig. 18. On the suction side laminar-turbulent transition is triggered at the injection location for both the single- and double-row configuration, resulting in a tremendous heat transfer augmentation of up to 3.5. Stronger mixing in the double row case gives values above those for the single row, especially in vicinity of the holes. Towards the trailing edge, where the boundary layer of the baseline tests is equally turbulent, no heat transfer augmentation is observed. On the pressure side, the boundary layer relaminarized downstream of injection, and transition occurs then towards the trailing edge, very similar to the baseline. A moderate heat transfer augmentation of 1.4 occurs at the pressure side injection location, but decreases rapidly to a value of 1 further downstream.
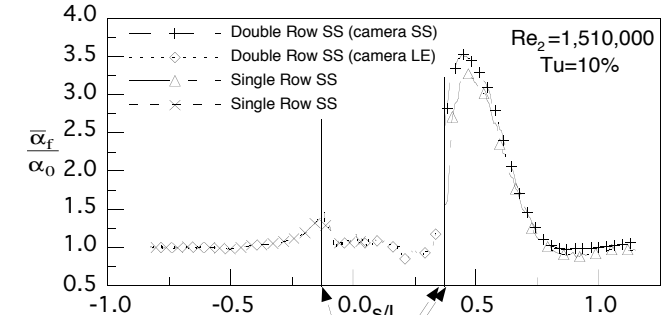

Fig. 18 Film Cooling heat transfer augmentation

Conclusions

• The transient liquid crystal technique has been successfully used for film cooling measurements on a flat plate and a turbine airfoil. A multiple-test regression method has been developed for the data reduction, considering a transient coolant temperature evolution.
• Flat plate film cooling effectiveness results compared well with published data for all momentum flux ratios, at low turbulence intensities. Heat transfer results were in good agreement for low momentum flux ratios, but showed increased values at higher coolant momentum.

- Mainstream turbulence reduces flat plate effectiveness at low and moderate blowing ratios, but increases the effectiveness at high blowing ratios due to a better dispersion of the detaching jets in the boundary layer.
- Film cooling measurements on a gas turbine airfoil at engine-representative conditions revealed a maximum effectiveness of 0.3 on the suction side with slightly higher values for the double row, but only low effectiveness on the pressure side. On the suction side, transition was initiated at the injection location.

ACKNOWLEDGMENTS

REFERENCES

Ammari , H.D., Hay, N., Lampard, D., 1990
The Effect of Density Ratio on the Heat Transfer Coefficient from a Film-Cooled Flat Plate.
ASME Transactions, Vol. 112, pp. 444-450
Baines, W.D., Peterson, E.G., 1951
An Investigation of Flow through Screens.
ASME Transactions, Vol. 73, pp. 467-480
Bajura, R.A., 1971
A Model for Flow Distribution in Manifolds
Journal of Engineering for Power, January 1971
Bendat, J.S., Piersol, A.G., 1986
Random Data, Analysis and Measurement Procedures
John Wiley & Sons 1986
von Doenhoff, A.E., Horton, E.A., 1956
A Low-Speed Experimental Investigation of the Effect of a Sandpaper Type of Roughness on Boundary Layer Transition
NACA Technical Note 3858
Eriksen, V.L., Goldstein, R.J., 1974
Heat Transfer and Film Cooling Following Injection Through Inclined Circular Tubes
Journal of Heat Transfer, May 1974, pp. 239-245
Forth, C.J.P, Loftus, P.J., Jones, T.V., 1985
The Effect of Density Ratio on the Film Cooling of a Flat Plate
AGARD CP 390, Bergen
Foster, N.W., Lampard, D., 1980
The Flow and Film Cooling Effectiveness Following Injection through a Row of Holes
Journal of Engineering for Power, July 1980, Vol. 102, pp. 584-588
Häring, M., Hoffs, A., Bölcs, A., 1995
An Experimental Study to Compare the Naphthalene with the Liquid Crystal Technique in Compressible Flow
ASME Paper 95-GT-16
Hoffs, A., Drost, U., Bölcs, A., 1996
Heat Transfer Measurements on a Turbine Airfoil at Various Reynolds Numbers and Turbulence Intensities Including Effects of Surface Roughness
ASME Paper 96-GT-169
Hoffs, A. 1996
Experimental Investigations of Heat Transfer and Film Cooling Effectiveness using the Transient Liquid Crystal Technique
Ph.D. Thesis, Swiss Federal Institute of Technology-Lausanne (EPFL)
Kline, S.J., McClintock, F.A., 1953
Describing Uncertainties in Single Sample Experiments
Mechanical Engineering, January 1953
Liess, C., 1975
Experimental Investigation of Film Cooling with Ejection from a Row of Holes for the Application to Gas Turbine Blades
Journal of Engineering for Power, Transaction of the ASME, January 1975
Ligrani, P.M., Camci, C., 1985
Adiabatic Film Cooling Effectiveness from Heat Transfer Measurements in Compressible, Variable-Property Flow
Journal of Heat Transfer, Vol.107, pp. 313-320
Schlichting, H., 1968
Boundary Layer Theory
6th ed., McGraw-Hill, New York
Schmidt, D.L., Bogard, D.G., 1996
Effects of Free-Stream Turbulence and Surface Roughness on Film Cooling
ASME Paper 96-GT-462
Schmidt, D.L., Sen, B., Bogard,D.G., 1994
Film Cooling with Compound Angle Holes: Adiabatic Effectiveness
ASME Paper 94-GT-312
Sinha, A.K., Bogard, D.G., Crawford, M.E., 1990
Film Cooling Effectiveness Downstream of a Single Row of Holes with Variable Density Ratio
ASME Paper 90-GT-43
Teekaram, A.J.H., Forth, C.J.P., Jones, T.V., 1989
The Use of Foreign Gas to Simulate the Effects of Density Ratios in Film Cooling
Journal of Turbomachinery, January 1989, Vol. 111, pp. 57-62
Teekaram, A.J.H., Forth, C.J.P., Jones, T.V., 1990
Film Cooling in the Presence of Mainstream Pressure Gradients
ASME Paper 90-GT-334
Vedula, R.,J., Metzger, D.E., 1991
A Method for the Simultanenous Determination of Local Effectiveness and Heat Transfer Distributions in Three-Temperature Convection Situations
ASME Paper 1991
Wang, Z., Ireland, P.T., Jones, T.V., 1994
A Colour Image Processing System for Transient Liquid Crystal Heat Transfer Experiments
ASME Paper 94-GT-290